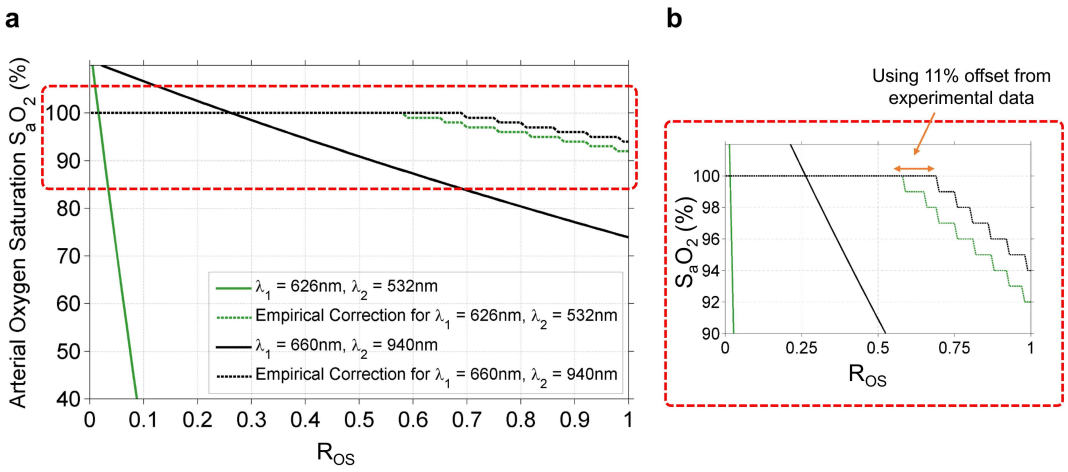

Supplementary Figure 1: **Arterial oxygen saturation (S_aO_2) as a function of transmitted light ratio (R_{OS}). a,** The `black solid line` shows the curve generated by Beer-Lambert's Law for red ($\lambda = 660$ nm) and infrared ($\lambda = 940$ nm) light. Similarly, the `green solid line` shows the curve generated by Beer-Lambert's Law for red ($\lambda = 626$ nm) and green ($\lambda = 532$ nm) light. Calibration curves to overcome limitations of Beer-Lambert's Law in scattering tissue (versus a glass cuvette) are shown by `dashed lines`. R_{OS} values were measured for various S_aO_2 values. **b**, We observed an 11% offset for the green light oximeter (`green dashed line`) from the conventional oximeter (`black dashed line`).

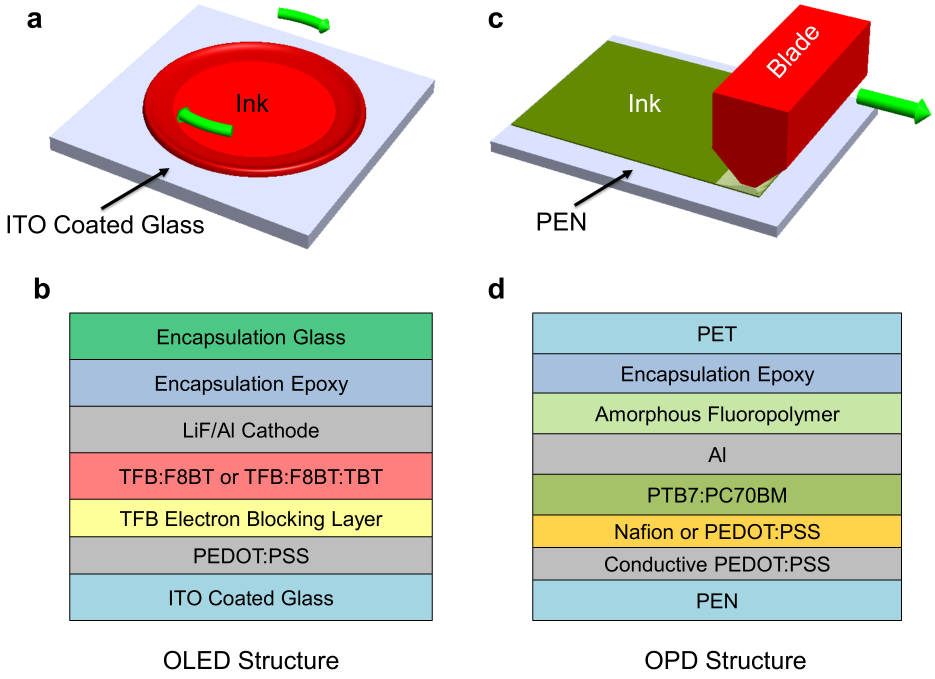

Supplementary Figure 2: **OLED and OPD fabrication and physical device structures. a**, The OLEDs are fabricated on a glass substrate using spin coating. **c**, The OPDs are fabricated using blade coating on a PEN substrate [4]. **b and d** respectively show the physical structures of the OLEDs and OPDs.

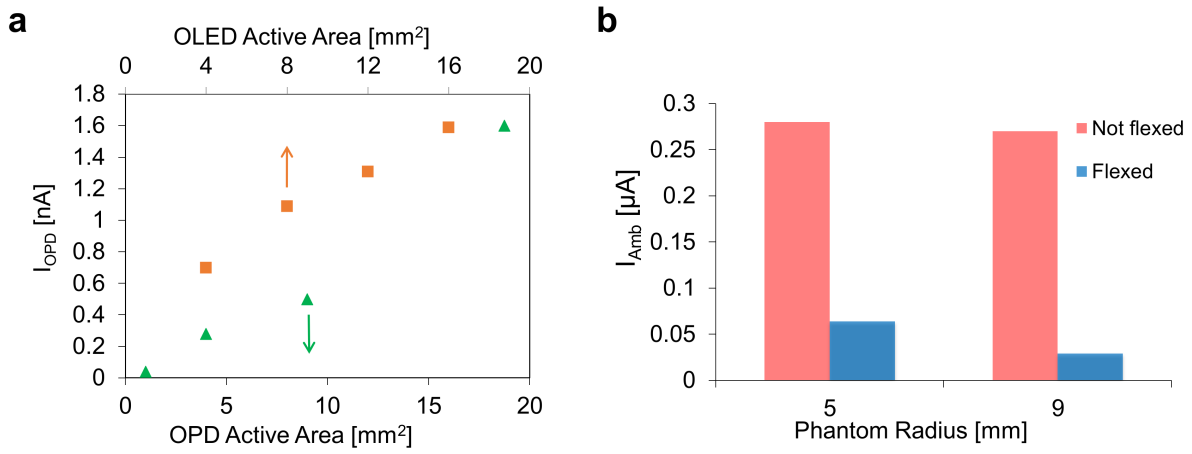

Supplementary Figure 3: **Area scaling effects of OLEDs and OPDs, and reducing ambient noise by flexing the OPD around a finger phantom. a,** OPD current (I_{OPD}) was observed for different OLED and OPD active areas. As expected, higher photo-current resulted with area scaling of the OLEDs and OPDs. **b**, OPDs were flexed around 5 mm and 9 mm radius phantoms representative of small and large human fingers. 79% and 93% reduction in ambient noise were observed for the OPDs flexed around the phantoms, respectively.

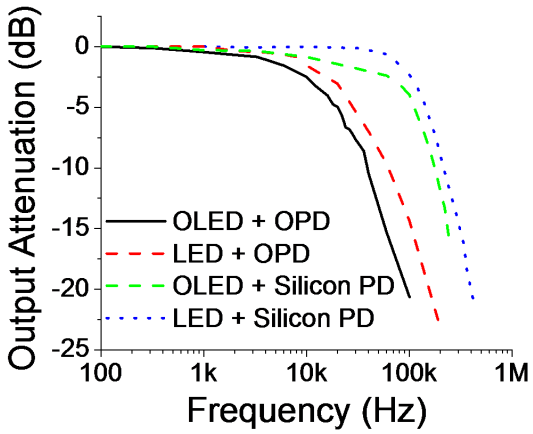

Supplementary Figure 4: **Frequency response of various organic and inorganic LED and PD configurations.** The inorganic LED and PD showed the best response with a 3dB cutoff greater than 100 kHz. For the all organic combination with OLED and OPD, 10 KHz cutoff was obtained, which is significantly higher than the 1 kHz operation of the oximeter. Green (λ = 532 nm) LEDs and OLEDs were used with a 5 V peak to peak sinusoidal signal and a DC offset of 2.5V.

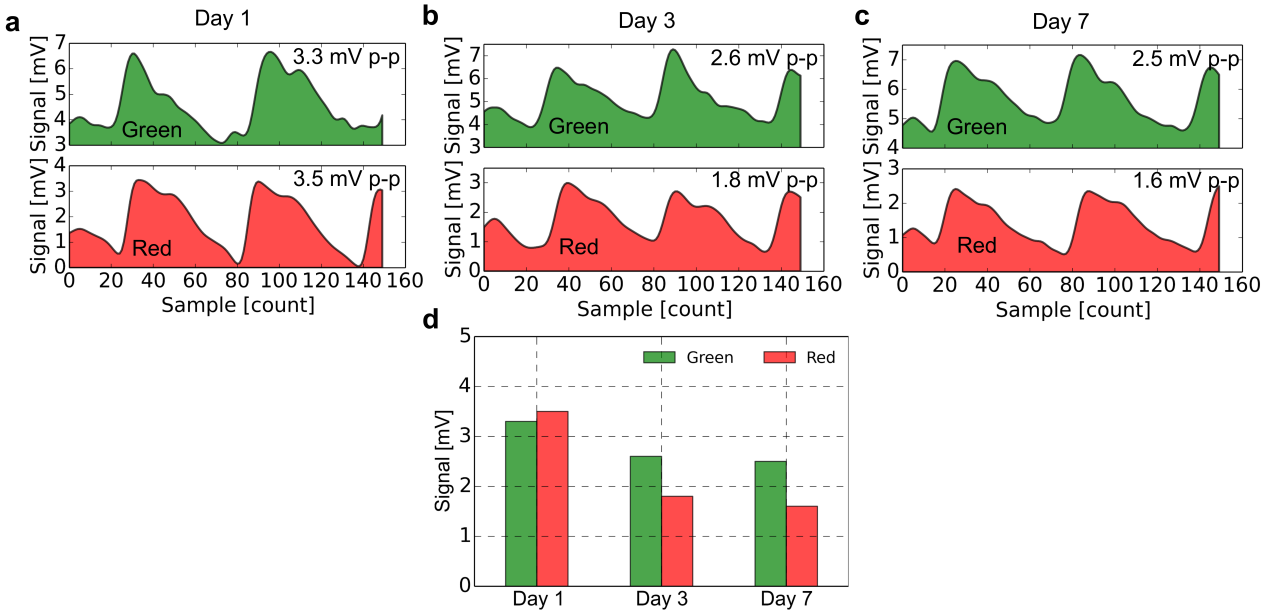

Supplementary Figure 5: **Stability of the all-organic optoelectronic sensor. a, b**, and **c**, Recorded signal intensities on day 1, 3, and 7 respectively after fabrication of the sensor. **d** Bar chart showing the degradation in signal intensity over seven day time period. Decline in performance is mainly due to encapsulation failure of the organic optoelectronics [5, 6].

I. SUPPLEMENTARY METHODS

A. Pulse oximetry using red and green OLEDs

In contrast to commercially available inorganic oximetry sensors, which use red and near-infrared LEDs, we used red and green OLEDs. We have replaced the near-infrared LED with a green OLED due to fact that solution-processable near-infrared OLEDs suffer from lower efficiencies. This substitution did not affect the pulse oximetry measurements because the difference in the molar extinction coefficient of oxygenated and deoxygenated hemoglobin at the green wavelength is comparable to the difference at near-infrared wavelengths. Conventionally, the saturation of oxygen in blood (SO_2) is quantified from the concentration of oxygenated hemoglobin C_{HbO_2} and the concentration of deoxygenated hemoglobin C_{Hb} [1–3]:

$$SO_2 = \frac{C_{HbO_2}}{C_{HbO_2} + C_{Hb}} \tag{1}$$

In transmission mode pulse oximetry, light from LEDs is directed into the top of the finger and the transmitted light is sensed at the bottom of the finger with a photodetector. Beer-Lambert's law states that the intensity of light traveling through a medium decreases exponentially with distance. Transmission T is given by,

$$T = I_0 \exp(-\varepsilon C d) \tag{2}$$

Here, I_0 is the incident light intensity, ε is the molar absorptivity with units of L $\mathrm{mM}^{-1}\mathrm{cm}^{-1}$, C is the concentration of the absorbent medium, and d is the optical path length through the medium.

The absorbance, A, is now defined as,

$$A = -\ln \frac{T}{I_0} = \varepsilon C d \tag{3}$$

Now if we consider attenuation in skin, tissue, and bones – represented with the subscript DC, and attenuation in oxy-hemoglobin and deoxy-hemoglobin – represented with the subscripts HbO_2 and Hb, the following equations represent transmission at diastole and systole:

$$T_{high,dia} = I_0 \exp(-\varepsilon_{DC} C_{DC} d_{DC}) \exp(-(\varepsilon_{HbO_2} C_{HbO_2} + \varepsilon_{Hb} C_{Hb}) d_{dia}) \tag{4}$$

$$T_{low,sys} = I_0 \exp(-\varepsilon_{DC} C_{DC} d_{DC}) \exp(-(\varepsilon_{HbO_2} C_{HbO_2} + \varepsilon_{Hb} C_{Hb}) d_{sys}) \tag{5}$$

Light has to pass through the additional optical path Δd at systole, therefore $d_{sys} = d_{dia} + \Delta d$. Additionally, a normalization step ($T_{normalized} = T/T_{high,dia}$) is required to determine the normalized systolic transmission.

Now Eq. 3 can be rewritten by superpositioning absorbance of HbO_2 and HbO at a specific wavelength,

$$A = (\varepsilon_{HbO_2} S_a O_2 + \varepsilon_{Hb}(1 - S_a O_2))(C_{HbO_2} + C_{Hb})\Delta d \tag{6}$$

The ratio of the absorbance at red (rd) and green (gr) light can be found using the following equation,

$$R_{os} = \frac{A_{rd}}{A_{gr}} = \frac{(\varepsilon_{rd,HbO_2} S_a O_2 + \varepsilon_{rd,Hb}(1 - S_a O_2))(C_{HbO_2} + C_{Hb})\Delta d}{(\varepsilon_{gr,HbO_2} S_a O_2 + \varepsilon_{gr,Hb}(1 - S_a O_2))(C_{HbO_2} + C_{Hb})\Delta d} \tag{7}$$

Finally, arterial oxygen saturation ($S_a O_2$) can be calculated using Eq. 8. Here, $\varepsilon_{rd,Hb}$ and $\varepsilon_{gr,Hb}$ are the molar absorptivity of deoxy-hemoglobin at red ($\lambda = 626$ nm) and green ($\lambda = 532$ nm) wavelengths. Similarly, ε_{rd,HbO_2} and ε_{gr,HbO_2} are the molar absorptivity of oxy-hemoglobin at red ($\lambda = 626$ nm) and green ($\lambda = 532$ nm) wavelengths.

$$S_a O_2(R_{os}) = \frac{\varepsilon_{rd,Hb} - \varepsilon_{gr,Hb} R_{os}}{(\varepsilon_{rd,Hb} - \varepsilon_{rd,HbO_2}) + (\varepsilon_{gr,HbO_2} - \varepsilon_{gr,Hb}) R_{os}} \tag{8}$$

$S_a O_2$ vs R_{os} for both red-infrared and red-green combinations are shown in Supplementary Figure 1a. However, empirical correction is required to overcome limitations of Beer-Lambert's Law in scattering tissue (versus a glass cuvette), which is given in Supplementary Figure 1b. We experimentally obtained the 11% offset in the calibration curves.

Supplementary References

[1] J. Webster, *Design of Pulse Oximeters*, Series in Medical Physics and Biomedical Engineering (Taylor & Francis, 2002), ISBN 9781420050790.

[2] M. Yelderman and W. New Jr, Anesthesiology **59**, 349 (1983).

[3] R. Haahr, M.S. thesis, Technical University of Denmark (2006).

[4] A. Pierre, M. Sadeghi, M. M. Payne, A. Facchetti, J. E. Anthony, and A. C. Arias, Advanced Materials **26**, 5722 (2014).

[5] J. Ahmad, K. Bazaka, L. J. Anderson, R. D. White, and M. V. Jacob, Renewable and Sustainable Energy Reviews **27**, 104 (2013).

[6] J.-S. Park, H. Chae, H. K. Chung, and S. I. Lee, Semiconductor Science and Technology **26**, 034001 (2011).